Journal of
Intelligent Material
Systems and Structures

*Original Article*

*Journal of Intelligent Material Systems and Structures*
1–15

DOI: 10.1177/1045389X221111545
journals.sagepub.com/home/jim
SAGE

# Recursive multiscale homogenization of multiphysics behavior of fuzzy fiber composites reinforced by hollow carbon nanotubes

**Qiang Chen, Fodil Meraghni and George Chatzigeorgiou**

**Abstract**

Fuzzy fibers are fibers enhanced in terms of multiphysics properties with radially oriented carbon nanotubes grown on their surface through the chemical deposition process. For the first time, this paper attempts to present two generalized zeroth-order asymptotic homogenization schemes aimed at identifying the homogenized and local response of fuzzy fiber-reinforced composites, accounting for both multiphysics piezoelectric effect and cylindrically orthotropic material behavior. The unit cell problems are solved using the multiphysics finite-volume and the multiphysics finite-element techniques, respectively. While the former approach is based on the strong form solution of the equilibrium and conservation equations in an averaged sense in the discretized domain, the latter is based on the minimization of the total potential energy over the entire unit cell. A recursive multiscale analysis algorithm is developed wherein homogenized moduli (or local fields) obtained from the homogenization (or localization) analysis at one scale are utilized in the calculation of homogenized moduli (or local fields) at the next scale. Numerical examples indicate that good agreement of the homogenized properties and local field distributions generated by the two approaches is observed hence confirming the accuracy of the new homogenization methods for fuzzy fiber composites with multiphysics behaviors.

**Keywords**

Fuzzy fiber composites, homogenization, piezoelectricity, multiphysics finite-volume method, multiphysics finite-element method

## 1. Introduction

Modern engineering applications require the development of composite materials with advanced mechanical, thermal, electric, etc., properties that provide high performances when employed for structural and/or functional components. Carbon nanotubes (CNTs) have shown excellent characteristics when introduced into composite structures (Aniskevich and Starkova, 2021; Ay and Tanoğlu, 2020; De Luca et al., 2020; Karger-Kocsis et al., 2020; Qian et al., 2010; Song et al., 2012). They are probably the strongest and stiffest materials that have been discovered with regard to the tensile strength and modulus. In a comparatively new type of "fuzzy" fiber composite materials, the CNTs are brought in by grafting and depositing on the fiber surfaces through the chemical vapor deposition, toward developing a new generation of composites with enhanced interfacial strength and stiffness, as shown in scanning electron microscopy (SEM) image (Figure 1), by Li et al. (2015).

The potential advantages obtained from the use of composites with enhanced fibers have fostered a tremendous interest in understanding the mechanical, thermal, and electric properties of such composites (Aravand et al., 2016; Aziz et al., 2015). Not only many experiments have been conducted in the literature in an effort of improving interphase behavior through fuzzy fiber technology (Aziz et al., 2015; Li et al., 2015; Qian et al., 2010; Yildiz et al., 2020), but also a few theoretical models are available to understand the micro/nanomechanics behaviors of fuzzy fiber composites, namely elastic (Chatzigeorgiou et al., 2011, 2012; Lurie et al., 2018; Rao et al., 2021); elastic-plastic (Chatzigeorgiou

Arts et Métiers Institute of Technology, CNRS, Université de Lorraine, Metz, France

**Corresponding author:**
George Chatzigeorgiou, Arts et Métiers Institute of Technology, CNRS, Université de Lorraine, LEM3-UMR7239, 4 Rue Augustin Fresnel, Metz F-57000, France.
Email: georges.chatzigeorgiou@ensam.eu

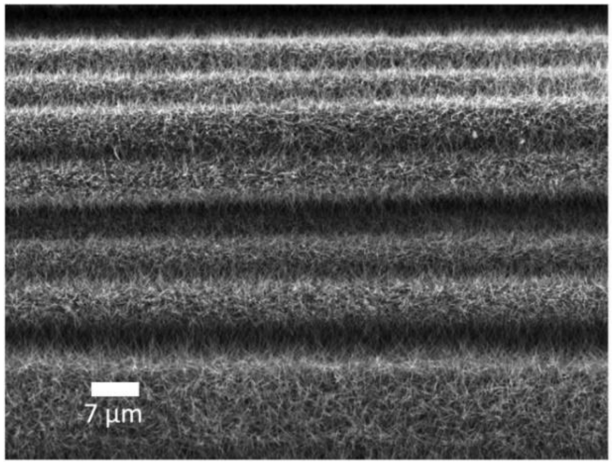


**Figure 1.** An SEM image of densely-packed carbon nanotube fibers on the fiber surface (Li et al., 2015). It is reprinted from the Composite Science and Technology, Vol. 117, "Hierarchical carbon nanotube carbon fiber unidirectional composites with preserved tensile and interfacial properties" by Richard Li, Noa Lachman, Peter Florin, H. Daniel Wagner, Brian L. Wardle, pp. 139–145, 2015, with permission from Elsevier.

et al., 2020; Chen et al., 2021); thermoelastic (Kundalwal and Ray, 2014); electromechanical (Dhala and Ray, 2015; Kundalwal et al., 2013). From the modeling point of view, the fuzzy fiber microstructures can be regarded as hierarchically reinforcing materials. First of all, the CNTs-reinforced interphase can be regarded as a nanocomposite made of radially-oriented carbon nanotubes embedded in the matrix. Following this spirit, the nanocomposite interphase is often treated as an equivalent homogeneous medium with cylindrically orthotropic multiphysics behaviors. For that reason, two concentric cylinders can be utilized to model the enhanced fibers, which represent the main fiber and the coated nanocomposites interphase (Chatzigeorgiou et al., 2020), respectively. As such, the fuzzy fiber microstructures are considered to be a three-scale medium, namely the microscale nanocomposite interphase (CNTs in the matrix), the mesoscale fuzzy fiber composites (fuzzy fiber in the matrix), and the macroscale composites.

Homogenization of fuzzy fiber composites with hierarchal microstructures relies on appropriate micromechanics tools, which can be solved in two steps. The first step of homogenization is conducted on the nanocomposite interphase in order to establish the effective properties of the equivalent interphase medium. The analytical solutions for fibers (solid or hollow fibers) embedded in a matrix allow for predicting effective elastic and thermal properties (Christensen and Lo, 1979; Hashin and Rosen, 1964). The classical micromechanics methods, such as the composite cylinder assemblage (CCA) model (Hashin and Rosen, 1964) and dilute approach (Isaeva and Topolov, 2021) continue to be appropriate tools for predicting the effective properties of hollow CNTs-reinforced nanocomposites. The recent extension of the CCA model by Chatzigeorgiou et al. (2019a, 2019b) has further enabled the efficient computation of homogenized properties of piezoelectric composites with an interphase layer. It should be noted that the classical micromechanics models are microstructural detail-free models. They contain either no direct information on the actual distribution of phases or account for their interaction in a rather simple manner (Pindera et al., 2009). What's more, the classical micromechanics models are based on the uniform stress or strain per phase, hence significantly underestimating the stress or strain concentration within the composite microstructures. While an accurate prediction of properties associated with the fiber axial direction may be obtained in light of the correct kinematic constraint, the effective properties in the transverse direction are generally quite inaccurate when the fiber/matrix property mismatch is remarkably large for realistic fiber volume fractions, such as the CNTs reinforced epoxy matrix. The advances in computing power have really enabled the computation of the homogenized properties using the more accurate full-field approaches such as finite-element and finite-volume-based approaches developed in this manuscript.

The homogenized properties of the nanocomposite interphase obtained in the first step are directly utilized for the prediction of the actual fuzzy fiber composites' effective behavior in the second step of homogenization. However, the presence of a cylindrically orthotropic interphase layer in composites adds notable complexity to the development of homogenization approaches with explicit expressions, since in the Cartesian coordinates of a standard unit cell the interphase is progressively functionally graded material whose properties are determined by their angular position and radial distance. This is particularly true in the case of the multiphysics effect, such as piezoelectricity. Analytical solutions for displacement field and electrical potential in the interphase layer are more difficult to derive compared to the pure mechanical case due to the electromechanical coupling and cylindrical orthotropic material behaviors. Therefore, in the second step of homogenization, these complicated heterogeneous materials cannot be studied with the classical multiscale methodologies. More sophisticated numerical homogenization methods are required to determine the homogenized properties of the overall composites in light of their flexibility to address complex microstructures and complicated constitutive law (Chen et al., 2018b; He and Pindera, 2021b; Kudimova et al., 2021).

The present paper proposes two novel zeroth-order asymptotic homogenization approaches for unidirectional fuzzy fiber composites accounting for the piezoelectric multiphysics effects. The fuzzy fiber composites studied herein consist of the active piezo ceramic fibers

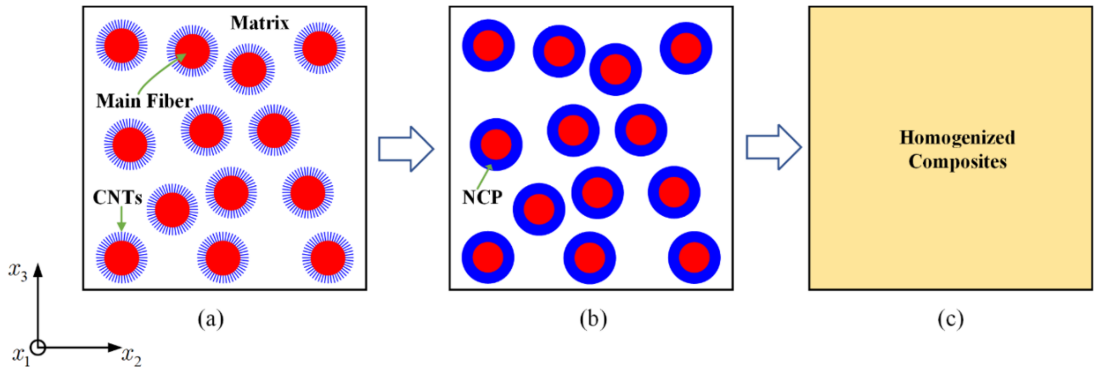


**Figure 2.** Hierarchical homogenization of the fuzzy fiber composites: (a) nanocomposite interphase, (b) fuzzy fiber composites, and (c) homogenized composites.

(Lead Zirconate Titanate) with grown CNTs which are embedded in a non-active epoxy matrix. The multiphysics finite-volume direct averaging micromechanics homogenization (MFVDAM) theory, detailed in Chen et al. (2018a), Tu and Chen (2021), is adopted and further extended to account for the cylindrically orthotropic material properties in the Cartesian coordinates. To validate the accuracy of the proposed MFVDAM, an in-house finite-element micromechanics code is also proposed considering the piezoelectric effect and cylindrically orthotopic constituent phases (Chen and Wang, 2020). Numerical results are generated by the two developed homogenization approaches, aiming at understanding the fundamental relationship between the micro/nanostructures, phase constituent properties, and their macroscopic behaviors. The main contributions of the present work include:

- construction of two novel multiphysics versions of finite-volume and finite-element homogenization techniques in the presence of cylindrically orthotropic phases
- comparison of predictive capacities of the multiphysics finite-volume and finite-element homogenization techniques for fuzzy fiber composites
- a thorough and comprehensive study of the homogenized and local behavior of fuzzy fiber composites under electro-mechanical loading at various scales

The remainder of the present work is organized as follows: Section 2 describes the problem under consideration and the generalized Hooke's law in different coordinate systems. Section 3 presents the theoretical framework for the multiphysics FVDAM and FEM micromechanics techniques. Parametric studies are conducted in Section 4 to investigate the effects of microstructural parameters and properties of constituent phases on the homogenized properties or local stress/electric concentrations within periodic arrays. Section 5 presents the discussion of the similarities and differences between the finite-volume and finite-element-based homogenization techniques. Figure 6 draws pertinent conclusions and future developments.

## 2. Fuzzy fiber composites with multiphysics effect

Figure 2(a) illustrates a schematic diagram of the representative fuzzy fiber composites with randomly dispersed infinitely-long main fibers that are coated by radially aligned hollow carbon nanotubes. Such composites can be regarded as a three-phase medium, namely, the main fiber, the matrix, and the nanocomposite interphase, as shown in Figure 2(b). The latter, which contains CNTs microfibers and the matrix, is considered as a homogenized coating layer encapsulating the main fiber. Accordingly, the following scales are found: the microscale involves the microfibers and the matrix; the mesoscale involves the main fiber, the matrix, and the equivalent nanocomposite interphase; and the macroscale is concerned with the homogenized fuzzy fiber composites.

As a result, the multiscale hierarchical homogenization scheme developed herein for such composites is conducted in two steps. The first step of the homogenization is performed on the CNTs microfibers and the surrounding matrix, in the cylindrical coordinate system, which yields the effective properties of nanocomposite interphase. In the second step of homogenization, the overall properties of the fuzzy fiber composites (Figure 2(c)) are obtained by homogenizing the matrix, main fiber, and the equivalent interlayer coating in the Cartesian coordinates.

The main fibers can be isotropic, transversely isotropic or orthotropic materials with the axis of symmetry parallel to the axis of the fibers. The nanocomposite interphase is treated as a cylindrically orthotropic material on account of the alignment of the microfibers in the radial direction. Due to the geometrical characteristics of the fuzzy fiber composites, the theoretical formulation of the homogenization theory is performed in two orthogonal coordinates, that is, the cylindrical

$(z, r, \theta)$ and Cartesian $(x_1, x_2, x_3)$ coordinates. The transformation relation between the two coordinate systems reads:

$$x_1 = z, \quad x_2 = r\cos\theta, \quad x_3 = r\sin\theta \tag{1}$$

Without loss of generality, let's consider the case where all the phases are fully anisotropic materials. The generalized constitutive relation of piezoelectric materials reads:

$$\begin{aligned} \boldsymbol{\sigma} &= \mathbf{C}\cdot\boldsymbol{\varepsilon} + \mathbf{e}\cdot[-\mathbf{E}] \\ \mathbf{D} &= \mathbf{e}^{\mathrm{T}}\cdot\boldsymbol{\varepsilon} - \boldsymbol{\kappa}\cdot[-\mathbf{E}] \end{aligned} \tag{2}$$

In compact form, $\boldsymbol{\Xi} = \mathbf{L}\cdot\mathbb{E}$, where $\boldsymbol{\Xi} = [\boldsymbol{\sigma},\ \mathbf{D}]^{\mathrm{T}}$, $\mathbb{E} = [\boldsymbol{\varepsilon},\ -\mathbf{E}]^{\mathrm{T}}$ and $\mathbf{L} = \begin{bmatrix} \mathbf{C} & \mathbf{e} \\ \mathbf{e}^{\mathrm{T}} & -\boldsymbol{\kappa} \end{bmatrix}$. $\boldsymbol{\sigma} = [\sigma_{11}, \sigma_{22}, \sigma_{33}, \sigma_{23}, \sigma_{13}, \sigma_{12}]^{\mathrm{T}}$ denotes stresses, $\boldsymbol{\varepsilon} = [\varepsilon_{11}, \varepsilon_{22}, \varepsilon_{33}, 2\varepsilon_{23}, 2\varepsilon_{13}, 2\varepsilon_{12}]^{\mathrm{T}}$ denotes strains, $\mathbf{D} = [D_1, D_2, D_3]^{\mathrm{T}}$ denotes electric displacements, $\mathbf{E} = [E_1, E_2, E_3]^{\mathrm{T}}$ denotes electric fields, $\mathbf{C} = \begin{bmatrix} C_{11} & C_{12} & C_{13} & C_{14} & C_{15} & C_{16} \\ C_{12} & C_{22} & C_{23} & C_{24} & C_{25} & C_{26} \\ C_{13} & C_{23} & C_{33} & C_{34} & C_{35} & C_{36} \\ C_{14} & C_{24} & C_{34} & C_{44} & C_{45} & C_{46} \\ C_{15} & C_{25} & C_{35} & C_{45} & C_{55} & C_{56} \\ C_{16} & C_{26} & C_{36} & C_{46} & C_{56} & C_{66} \end{bmatrix}$ denotes the elastic stiffness, $\mathbf{e} = \begin{bmatrix} e_{11} & e_{21} & e_{31} \\ e_{12} & e_{22} & e_{32} \\ e_{13} & e_{23} & e_{33} \\ e_{14} & e_{24} & e_{34} \\ e_{15} & e_{25} & e_{35} \\ e_{16} & e_{26} & e_{36} \end{bmatrix}$ and $\boldsymbol{\kappa} = \begin{bmatrix} \kappa_{11} & \kappa_{12} & \kappa_{13} \\ \kappa_{12} & \kappa_{22} & \kappa_{23} \\ \kappa_{13} & \kappa_{23} & \kappa_{33} \end{bmatrix}$ are the piezoelectric and dielectric properties written in matrices using the Voigt notation.

In Voigt notation, the stress, strain, electric displacement, and electric fields are transformed between the cylindrical (indicated by the tilde symbol) and Cartesian coordinate systems through the matrix-type formulas (Chatzigeorgiou et al., 2017):

$$\begin{aligned} &\tilde{\boldsymbol{\varepsilon}} = \mathbf{Q}_{\varepsilon}\cdot\boldsymbol{\varepsilon}, \quad \tilde{\boldsymbol{\sigma}} = \mathbf{Q}_{\sigma}\cdot\boldsymbol{\sigma}, \quad \boldsymbol{\varepsilon} = \mathbf{Q}_{\sigma}^{\mathrm{T}}\cdot\tilde{\boldsymbol{\varepsilon}}, \quad \boldsymbol{\sigma} = \mathbf{Q}_{\varepsilon}^{\mathrm{T}}\cdot\tilde{\boldsymbol{\sigma}}, \\ &\tilde{\mathbf{E}} = \mathbf{R}^{\mathrm{T}}\cdot\mathbf{E}, \quad \tilde{\mathbf{D}} = \mathbf{R}^{\mathrm{T}}\cdot\mathbf{D}, \quad \mathbf{E} = \mathbf{R}\cdot\tilde{\mathbf{E}}, \quad \mathbf{D} = \mathbf{R}\cdot\tilde{\mathbf{D}} \end{aligned} \tag{3}$$

where $\tilde{\boldsymbol{\sigma}} = [\sigma_{zz}, \sigma_{rr}, \sigma_{\theta\theta}, \sigma_{r\theta}, \sigma_{z\theta}, \sigma_{zr}]^{\mathrm{T}}$, $\tilde{\boldsymbol{\varepsilon}} = [\varepsilon_{zz}, \varepsilon_{rr}, \varepsilon_{\theta\theta}, 2\varepsilon_{r\theta}, 2\varepsilon_{z\theta}, 2\varepsilon_{zr}]^{\mathrm{T}}$, $\tilde{\mathbf{D}} = [D_z, D_r, D_\theta]^{\mathrm{T}}$, $\tilde{\mathbf{E}} = [E_z, E_r, E_\theta]^{\mathrm{T}}$ respectively are stresses, strains, electric displacements and electric fields in the cylindrical coordinates. $\mathbf{R}$ represents the rotator second-order tensor. Given the equation (1), it reads:

$$\mathbf{R} = \begin{bmatrix} 1 & 0 & 0 \\ 0 & \cos\theta & -\sin\theta \\ 0 & \sin\theta & \cos\theta \end{bmatrix} \tag{4}$$

$\mathbf{Q}_{\varepsilon}$ and $\mathbf{Q}_{\sigma}$ are the proper fourth-order rotators that transform the strain and the stress vectors expressed in Voigt notation (Chatzigeorgiou et al., 2017), respectively:

$$\mathbf{Q}_{\varepsilon} = \begin{bmatrix} 1 & 0 & 0 & 0 & 0 & 0 \\ 0 & \cos^2\theta & \sin^2\theta & \cos\theta\sin\theta & 0 & 0 \\ 0 & \sin^2\theta & \cos^2\theta & -\cos\theta\sin\theta & 0 & 0 \\ 0 & -2\cos\theta\sin\theta & 2\cos\theta\sin\theta & \cos^2\theta - \sin^2\theta & 0 & 0 \\ 0 & 0 & 0 & 0 & \cos\theta & -\sin\theta \\ 0 & 0 & 0 & 0 & \sin\theta & \cos\theta \end{bmatrix} \tag{5}$$

$$\mathbf{Q}_{\sigma} = \begin{bmatrix} 1 & 0 & 0 & 0 & 0 & 0 \\ 0 & \cos^2\theta & \sin^2\theta & 2\cos\theta\sin\theta & 0 & 0 \\ 0 & \sin^2\theta & \cos^2\theta & -2\cos\theta\sin\theta & 0 & 0 \\ 0 & -\cos\theta\sin\theta & \cos\theta\sin\theta & \cos^2\theta - \sin^2\theta & 0 & 0 \\ 0 & 0 & 0 & 0 & \cos\theta & -\sin\theta \\ 0 & 0 & 0 & 0 & \sin\theta & \cos\theta \end{bmatrix} \tag{6}$$

With the help of the above rotators, the transformation of the generalized stiffness matrix between the cylindrical and Cartesian coordinates takes the form:

$$\tilde{\mathbf{L}} = \mathbf{W}_{\Xi}\cdot\mathbf{L}\cdot\mathbf{W}_{\Xi}^{\mathrm{T}} \qquad \mathbf{L} = \mathbf{W}_{E}^{\mathrm{T}}\cdot\tilde{\mathbf{L}}\cdot\mathbf{W}_{E} \tag{7}$$

where

$$\mathbf{W}_{\Xi} = \begin{bmatrix} \mathbf{Q}_{\sigma} & \mathbf{0} \\ \mathbf{0} & \mathbf{R}^{\mathrm{T}} \end{bmatrix} \qquad \mathbf{W}_{E} = \begin{bmatrix} \mathbf{Q}_{\varepsilon} & \mathbf{0} \\ \mathbf{0} & \mathbf{R}^{\mathrm{T}} \end{bmatrix}$$

To accurately capture the effective properties of the overall fuzzy fiber composites, a suitable micromechanics scheme with multiphysics capability needs to be developed. The cylindrical microstructures of the nanocomposite interphase pose challenges in terms of

homogenization of multiphysics behaviors in the Cartesian coordinates. First of all, at the first step of homogenization (microscale), the nanocomposite interphase with radially aligned CNTs cannot be replicated by the duplication of the same unit cell, as in the Cartesian periodic homogenization. Therefore, the unit cell problem should be formulated considering cylindrical periodicity (Tsalis et al., 2012). A complication related to homogenization with the cylindrical periodicity is the fact that the volume fraction of the CNTs decreases in a progressive manner with increasing radial distance, leading to a progressively functionally graded effective coating layer at the mesoscale. Finally, the homogenized properties of the nanocomposite interphase exhibit cylindrically orthotropic material behaviors. At the second step of homogenization (mesoscale), the generalized effective stiffness tensor of the coating layer expressed in the Cartesian coordinates depends on the angular position and radial distance.

From a computational point of view, to capture the progressively graded effective properties in the nanocomposite interphase, the microscale homogenization needs to be conducted for several unit cells along the radial direction, whose effective properties are analyzed numerically to take into account the variation of the CNTs volume fractions at different radial distances. In the present manuscript, in a coarse but successful approximation, we assume the nanocomposite interphase acts like a classical unidirectional composite hence only one interphase layer is utilized to compute their effective behaviors. The effective properties of the CNTs (hollow microfibers) reinforced unidirectional composites can be identified through either numerical or analytical homogenization strategies. The effective properties of the nanocomposites in the cylindrical coordinates are then transformed to their Cartesian counterparts in order to perform numerically the mesoscale homogenization.

## 3. Theoretical developments

The multiphysics micromechanics approaches based on the multiphysics finite-volume direct averaging micromechanics (MFVDAM) and the multiphysics finite-element micromechanics (MFEM) homogenization theories have been developed by (Chen and Wang, 2020; Chen et al., 2018a). Hereinafter, they are further extended to account for cylindrically orthotopic phases and are utilized to obtain the homogenized and local behaviors at both micro- and mesoscales of the fuzzy fiber composites.

In the multiphysics FVDAM theory, the repeating unit cell representative of a unidirectional composite is discretized into quadrilateral subvolumes designated by the index $(q)$ whose location is specified by the vertices subvolume vertices $(y_2, y_3)^{(p,q)}$. Following Cavalcante et al. (2007), the vertices of the $q$th subvolume are numbered in a counter-clockwise manner starting from the lower-left corner $(y_2, y_3)^{(1,q)}$. Consistently the face $F_p$ denotes the subvolume face defined by the endpoints $(y_2, y_3)^{(p,q)}$ and $(y_2, y_3)^{(p+1,q)}$, and when $p = 4$, $p + 1 \rightarrow 1$. The $q$th subvolume situated in the physical domain $(y_2 - y_3)$ is created by mapping the reference square in the $(\eta - \xi)$ plane bounded by $-1 \leqslant \eta \leqslant +1$ and $-1 \leqslant \xi \leqslant +1$ onto its actual locations in the unit cell using the parametric mapping:

$$y_i^{(q)}(\eta, \xi) = \sum_{p=1}^{m} N_p(\eta, \xi) y_i^{(p,q)}, \quad i = 2, 3 \tag{8}$$

where $m$ denotes the node number. For the MFVDAM, $m = 4$, and

$$\begin{aligned} N_1(\eta, \xi) &= \frac{1}{4}(1 - \eta)(1 - \xi), \\ N_2(\eta, \xi) &= \frac{1}{4}(1 + \eta)(1 - \xi), \\ N_3(\eta, \xi) &= \frac{1}{4}(1 + \eta)(1 + \xi), \\ N_4(\eta, \xi) &= \frac{1}{4}(1 - \eta)(1 + \xi) \end{aligned}$$

In contrast, in the case of multiphysics FEM analysis, the 8-noded parametric mapping is employed to obtain the $q$th element in the actual coordinates. $(y_2, y_3)^{(p,q)}$ designated by the index $p$ are the coordinates at the four corners and four midpoints of the reference element starting at the lower-left corner and progressing counterclockwise. The mapping functions are given by:

$$\begin{aligned} N_1(\eta, \xi) &= -\frac{1}{4}(1 - \eta)(1 - \xi)(1 + \eta + \xi), \\ N_5(\eta, \xi) &= \frac{1}{2}\left(1 - \eta^2\right)(1 - \xi) \\ N_2(\eta, \xi) &= -\frac{1}{4}(1 + \eta)(1 - \xi)(1 - \eta + \xi), \\ N_6(\eta, \xi) &= \frac{1}{2}(1 + \eta)\left(1 - \xi^2\right) \\ N_3(\eta, \xi) &= -\frac{1}{4}(1 + \eta)(1 + \xi)(1 - \eta - \xi), \\ N_7(\eta, \xi) &= \frac{1}{2}\left(1 - \eta^2\right)(1 + \xi) \\ N_4(\eta, \xi) &= -\frac{1}{4}(1 - \eta)(1 + \xi)(1 + \eta - \xi), \\ N_8(\eta, \xi) &= \frac{1}{2}(1 - \eta)\left(1 - \xi^2\right) \end{aligned} \tag{9}$$

The MFVDAM and MFEM provide a coherent framework to account for the variation of macroscopic strain and electric fields in microstructures which are distributed in a periodical manner in the lower scale. The unit cell problems are solved subject to periodic boundary conditions. Following the asymptotic

expansion theory widely used in the homogenization theory of composites (Chen et al., 2018b; He and Pindera, 2021a, 2021b; Yang and Müller, 2021; Yang et al., 2020; Zhi et al., 2021a, 2021b), the displacement and electric potential fields are represented by the two-scale expansion involving the macroscopic coordinates $\mathbf{x}$ and the microscopic coordinates $\mathbf{y}$ of the following form:

$$u_i^{(q)}(\mathbf{x},\mathbf{y}) = \bar{\varepsilon}_{ij}x_j + u_i'^{(q)}(\mathbf{y}) \quad \alpha^{(q)}(\mathbf{x},\mathbf{y}) = -\bar{E}_i x_i + \alpha'^{(q)}(\mathbf{y}) \tag{10}$$

where $i = 1,2,3$, $\bar{\varepsilon}_{ij}$ is the applied macroscopic strain and $\bar{E}_i$ is the applied macroscopic electric field. $u_i'(q)$ and $\alpha'^{(q)}$ denote the fluctuating displacement and electric potential fields induced by the microstructures. Accordingly, the microscopic strain $\varepsilon_{ij}^{(q)}$ and electric fields $E_i^{(q)}$ are obtained in terms of macroscopic and fluctuating components as follows:

$$\begin{aligned} \varepsilon_{ij}^{(q)} &= \bar{\varepsilon}_{ij} + \varepsilon_{ij}'^{(q)} = \bar{\varepsilon}_{ij} + \frac{1}{2}\left(\frac{\partial u'_i}{\partial y_j} + \frac{\partial u'_j}{\partial y_i}\right)^{(q)} \\ E_i^{(q)} &= \bar{E}_i + E_i'^{(q)} = \bar{E}_i - \frac{\partial \alpha'^{(q)}}{\partial y_i} \end{aligned} \tag{11}$$

### 3.1. Finite-volume based solution

In the multiphysics FVDAM theory, the fluctuating displacements and electric potentials are represented by the second-order Legendre polynomial expression in the reference coordinates $(\eta,\xi)$:

$$\begin{aligned} u_i'(q) &= W_{i(00)}^{(q)} + \eta W_{i(10)}^{(q)} + \xi W_{i(01)}^{(q)} + \frac{1}{2}\left(3\eta^2-1\right)W_{i(20)}^{(q)} \\ &\quad + \frac{1}{2}\left(3\xi^2-1\right)W_{i(02)}^{(q)}, \quad i = 1,2,3 \\ \alpha'^{(q)} &= W_{4(00)}^{(q)} + \eta W_{4(10)}^{(q)} + \xi W_{4(01)}^{(q)} + \frac{1}{2}\left(3\eta^2-1\right)W_{4(20)}^{(q)} \\ &\quad + \frac{1}{2}\left(3\xi^2-1\right)W_{4(02)}^{(q)} \end{aligned} \tag{12}$$

where $W_{i(mn)}^{(q)}$ are the unknown microscopic variables associated with each subvolume. Ultimately, these unknown coefficients will be related to surface-averaged displacements and electric potentials, upon solving the local equilibrium and conservation equations.

Following the classical development of the finite-volume theory, the surface-averaged fluctuating displacements $\hat{u}_i'^{(p,q)}$, electric potentials $\hat{\alpha}'^{(p,q)}$, and the surface-averaged tractions $\hat{t}_i^{(p,q)}$ and electric displacements $\hat{D}^{(p,q)}$, defined as follows, are used in the construction of the generalized local stiffness matrices:

For $p = 1,3$,

$$\begin{aligned} \hat{u}_i^{(p,q)} &= \frac{1}{2}\int_{-1}^{+1} u'_i(\eta,\mp 1)d\eta, \\ \hat{\alpha}'^{(p,q)} &= \frac{1}{2}\int_{-1}^{+1} \alpha'(\eta,\mp 1)d\eta \\ \hat{t}_i^{(p,q)} &= \frac{1}{2}\int_{-1}^{+1} \sigma_{ij}(\eta,\mp 1)\cdot n_j d\eta, \\ \hat{D}^{(p,q)} &= \frac{1}{2}\int_{-1}^{+1} D_i(\eta,\mp 1)\cdot n_i d\eta \end{aligned} \tag{13}$$

For $p = 2,4$,

$$\begin{aligned} \hat{u}_i^{(p,q)} &= \frac{1}{2}\int_{-1}^{+1} u'_i(\pm 1,\xi)d\xi, \\ \hat{\alpha}'^{(p,q)} &= \frac{1}{2}\int_{-1}^{+1} \alpha'(\pm 1,\xi)d\xi \\ \hat{t}_i^{(p,q)} &= \frac{1}{2}\int_{-1}^{+1} \sigma_{ij}(\pm 1,\xi)\cdot n_j d\xi, \\ \hat{D}^{(p,q)} &= \frac{1}{2}\int_{-1}^{+1} D_i(\pm 1,\xi)\cdot n_i d\xi \end{aligned} \tag{14}$$

where $\mathbf{n} = [n_2, n_3]$ denotes the unit normal vector defining the orientations of each face.

To obtain the generalized local stiffness matrices, the microvariables $W_{i(mn)}^{(q)}$ in the displacement and electric potential field representations must be expressed in terms of fluctuating surface-averaged displacements and electric potentials. Using the definition in equations (13) and (14), the first- $W_{i(10)}^{(q)}, W_{i(01)}^{(q)}$ and second-order $W_{i(20)}^{(q)}, W_{i(02)}^{(q)}$ unknown coefficients are first expressed in terms of the fluctuating surface-averaged displacements $\hat{u}_i'^{(p,q)}$, electric potentials $\hat{\alpha}'^{(p,q)}$ and the zeroth-order coefficients $W_{i(00)}^{(q)}$. Subsequently, the satisfaction of the stress equilibrium and the Maxwell conservation conditions in the large produces four equations for the determination of the zeroth-order coefficients $W_{i(00)}^{(q)}$:

$$\begin{aligned} \int_{S_q} \sigma_{ij}n_j dS &= \sum_{p=1}^{4} l^{(p,q)}\hat{t}_i^{(p,q)} = 0 \\ \int_{S_q} D_i n_i dS &= \sum_{p=1}^{4} l^{(p,q)}\hat{D}^{(p,q)} = 0 \end{aligned} \tag{15}$$

where $l^{(p,q)}$ denotes the length of the $p$th face of the $q$th subvolume.

The ultimate relations between the surface-averaged tractions, electric displacements, and the mechanical displacements, electric potentials can be written in the matrix and vector forms as (with $q$ omitted for simplification):

$$\bar{\boldsymbol{\Xi}} = \mathbf{K}\cdot\hat{\boldsymbol{\Sigma}}' + \mathbf{N}\cdot\mathbf{L}\cdot\bar{\mathbb{E}} \tag{16}$$

In the above equation,

$$\bar{\boldsymbol{\Xi}} = \left[\hat{\mathbf{q}}^{(1)}, \hat{\mathbf{q}}^{(2)}, \hat{\mathbf{q}}^{(3)}, \hat{\mathbf{q}}^{(4)}\right]^{\mathrm{T}} \text{with } \hat{\mathbf{q}}^{(p)} = \left[\hat{t}_1, \hat{t}_2, \hat{t}_3, \hat{D}\right]^{(p)^{\mathrm{T}}},$$

$$\hat{\boldsymbol{\Sigma}}' = \left[\mathbf{r}^{(1)}, \mathbf{r}^{(2)}, \mathbf{r}^{(3)}, \mathbf{r}^{(4)}\right]^{\mathrm{T}} \text{with } \hat{\mathbf{r}}^{(p)} = \left[\hat{u}'_1, \hat{u}'_2, \hat{u}'_3, \hat{\alpha}'\right]^{(p)^{\mathrm{T}}},$$

$$\mathbf{N} = \left[\mathbf{n}^{(1)}, \mathbf{n}^{(2)}, \mathbf{n}^{(3)}, \mathbf{n}^{(4)}\right]^{(\mathrm{T})} \text{with } \mathbf{n}^{(p)} = \begin{bmatrix} 0 & 0 & 0 & 0 & n_3 & n_2 & 0 & 0 & 0 \\ 0 & n_2 & 0 & n_3 & 0 & 0 & 0 & 0 & 0 \\ 0 & 0 & n_3 & n_2 & 0 & 0 & 0 & 0 & 0 \\ 0 & 0 & 0 & 0 & 0 & 0 & 0 & n_2 & n_3 \end{bmatrix}^{(p)},$$

and $\mathbf{K}$ denotes the local stiffness matrices which are derived explicitly in terms of subvolume geometry and generalized stiffness occupying the $q$th subvolume.

The unknown interfacial mechanical displacements and electric potentials are determined by solving a global system of equations obtained by the enforcement of traction and electric displacement continuity and periodicity conditions, followed by direct enforcement of mechanical displacement and electric potential continuity and periodicity conditions. The resulting system of equations can be expressed in compact form as follows:

$$\mathbb{K} \cdot \hat{\mathbb{U}}' = \Delta\mathbb{L} \cdot \bar{\mathbb{E}} \tag{17}$$

where $\mathbb{K}$ denotes the global stiffness matrix, $\hat{\mathbb{U}}'$ contains all the unknown interfacial surface-averaged mechanical displacements and electric potentials. $\Delta\mathbb{L}$ represents the differences in the generalized stiffness matrices of adjacent subvolumes.

### 3.2. Finite-element based solution

In the multiphysics FEM homogenization, the fluctuating displacements and electric potentials are approximated using the Q8-element shape functions given directly in terms of nodal quantities and interpolation functions:

$$\begin{aligned} u_i'^{(q)}(\eta, \xi) &= \sum_{p=1}^{m} N_p(\eta, \xi) u_i^{'o(p,q)}, \quad i = 1, 2, 3 \\ \alpha'^{(q)}(\eta, \xi) &= \sum_{p=1}^{m} N_p(\eta, \xi) \alpha'^{o(p,q)} \end{aligned} \tag{18}$$

where $u_i^{'o(p,q)}$ and $\alpha'^{o(p,q)}$ are the nodal displacements and electric potentials respectively. For direct comparison with the MFVDAM theory, the fluctuating displacements and electric potential for the Q8 elements may be written as:

$$\begin{aligned} u_i'(q) &= U_{i(00)}^{(q)} + \eta U_{i(10)}^{(q)} + \xi U_{i(01)}^{(q)} + \eta\xi U_{i(11)}^{(q)} + \eta^2 U_{i(20)}^{(q)} \\ &\quad + \xi^2 U_{i(02)}^{(q)} + \eta^2\xi U_{i(21)}^{(q)} + \eta\xi^2 U_{i(12)}^{(q)} \\ \alpha'^{(q)} &= U_{4(00)}^{(q)} + \eta U_{4(10)}^{(q)} + \xi U_{4(01)}^{(q)} + \eta\xi U_{4(11)}^{(q)} + \eta^2 U_{4(20)}^{(q)} \\ &\quad + \xi^2 U_{4(02)}^{(q)} + \eta^2\xi U_{4(21)}^{(q)} + \eta\xi^2 U_{4(12)}^{(q)} \end{aligned} \tag{19}$$

where $U_{i(mn)}^{(q)}$ are the unknown microvariables. Applying the differential operators to the internal trial displacements and electric potential, the fluctuating strain and electric fields are obtained in the following form:

$$\boldsymbol{\varepsilon}'^{(q)} = \mathbf{B}_u^{(q)} \mathbf{u}'^{o(q)} \qquad \mathbf{E}'^{(q)} = -\mathbf{B}_\alpha^{(q)} \boldsymbol{\alpha}'^{o(q)} \tag{20}$$

where $\mathbf{u}'^{o(q)} = [\mathbf{u}'^{(1)} \ldots \mathbf{u}'^{(8)}]^{\mathrm{T}}$ and $\mathbf{u}'^{(p)} = [u'_1, u'_2, u'_3]^{o(p)\mathrm{T}}$. $\boldsymbol{\alpha}'^{o(q)} = \left[\alpha^{(1)}, \ldots, \alpha^{(8)}\right]^{\mathrm{T}}$. $\mathbf{B}_u^{(q)}$ denotes the strain-displacement relation and $\mathbf{B}_\alpha^{(q)}$ denotes the electric field-electric potential relation, which are used to construct the potential energy integral at the element level.

The total potential energy of the unit cell is obtained from the summation of the bulk strain and electric energies, as well as the work done by the external force and electric charge:

$$\begin{aligned} \Pi = U^b - W = \frac{1}{2}\int_V \left(\boldsymbol{\sigma}^{\mathrm{T}} \cdot \boldsymbol{\varepsilon} - \mathbf{D}^{\mathrm{T}} \cdot \mathbf{E}\right) \mathrm{d}V \\ -(\bar{\boldsymbol{\sigma}}^{\mathrm{T}} \cdot \bar{\boldsymbol{\varepsilon}} - \bar{\mathbf{D}}^{\mathrm{T}} \cdot \bar{\mathbf{E}}) V \end{aligned} \tag{21}$$

The generalized local stiffness matrices are obtained by the minimization of total potential energy equation (21), which is done by substituting equations (11) and (20) into equation (21) with the help of the generalized Hooke's law and then making the first variations:

$$\begin{bmatrix} \mathbf{K}_{uu} & \mathbf{K}_{u\alpha} \\ \mathbf{K}_{u\alpha}^{\mathrm{T}} & \mathbf{K}_{\alpha\alpha} \end{bmatrix} \begin{bmatrix} \mathbf{u}'^{\mathrm{o}} \\ \boldsymbol{\alpha}'^{\mathrm{o}} \end{bmatrix} = \begin{bmatrix} \mathbf{f}_u \\ \mathbf{f}_\alpha \end{bmatrix} \tag{22}$$

where $\mathbf{K}_{uu} = \int_V \mathbf{B}_u^{\mathrm{T}} \mathbf{C} \mathbf{B}_u \mathrm{d}V$, $\mathbf{K}_{\alpha\alpha} = -\int_V \mathbf{B}_\alpha^T \boldsymbol{\kappa} \mathbf{B}_\alpha \mathrm{d}V$, $\mathbf{K}_{u\alpha} = \int_V \mathbf{B}_u^{\mathrm{T}} \mathbf{e} \mathbf{B}_\alpha \mathrm{d}V$, $\mathbf{f}_u = \int_V (\mathbf{B}_u^{\mathrm{T}} \mathbf{e} \bar{\mathbf{E}} - \mathbf{B}_u^{\mathrm{T}} \mathbf{C} \bar{\boldsymbol{\varepsilon}}) \mathrm{d}V$, $\mathbf{f}_\alpha = -\int_V (\mathbf{B}_\alpha^{\mathrm{T}} \mathbf{e}^{\mathrm{T}} \bar{\boldsymbol{\varepsilon}} + \mathbf{B}_\alpha^{\mathrm{T}} \boldsymbol{\kappa} \bar{\mathbf{E}}) \mathrm{d}V$.

The local stiffness matrices are assembled into a global system of equations by enforcing the continuities of displacements and electric potentials at common nodes of adjacent elements, as well as the periodicity conditions at the mirrored faces of a repeating unit cell. The final form of the system of equations for the determination of the nodal displacements and electric potentials can be expressed in the following symbolic form:

$$\begin{bmatrix} \mathbb{K}_{uu} & \mathbb{K}_{u\alpha} \\ \mathbb{K}_{u\alpha}^{\mathrm{T}} & \mathbb{K}_{\alpha\alpha} \end{bmatrix} \begin{bmatrix} \mathbb{U}' \\ \boldsymbol{\alpha}' \end{bmatrix} = \begin{bmatrix} \mathbb{F}_u \\ \mathbb{F}_\alpha \end{bmatrix} \tag{23}$$

### 3.3. Homogenized generalized stiffness matrix

The homogenized generalized stiffness matrix $\mathbf{L}^*$ of the unit cell is obtained by sequentially applying one unit strain or electric field to solve the equations (17) and (23) iteratively nine times for the surface-averaged unknown vector $\hat{\mathbb{U}}'$ or the nodal displacements $\mathbb{U}'$ and electrical potentials $\boldsymbol{\alpha}'$, hence the stress and electric displacement fields. The macroscopic loading conditions for a specific boundary value problem are applied through the homogenized strains or electric fields directly. For instance, in order to obtain the first column in the generalized homogenized stiffness tensor, the following loading condition is applied:

$$\bar{\mathbb{E}} = [1, 0, 0, 0, 0, 0, 0, 0, 0]^{\mathrm{T}}$$

As a result, the solution of the global system of equations yields nine components of macroscopic stresses and electric displacements through the volume-averaging of their corresponding local fields over the entire unit cell volume $V$:

$$\bar{\sigma}_{ij} = \frac{1}{V}\int_V \sigma_{ij}\mathrm{d}V, \quad \bar{D}_i = \frac{1}{V}\int_V D_i\mathrm{d}V \tag{24}$$

which are respectively equal to the elements in the first column of $\mathbf{L}^*$, that is, $C^*_{11}, C^*_{21}, C^*_{31}, C^*_{41}, C^*_{51}, C^*_{61}$, $e^*_{11}, e^*_{21}, e^*_{31}$. Similarly, the second column of $\mathbf{L}^*$ can be obtained by applying:

$$\bar{\mathbb{E}} = [0, 1, 0, 0, 0, 0, 0, 0, 0]^{\mathrm{T}}$$

This procedure is continued till all the columns of $\mathbf{L}^*$ have been obtained.

Finally, using equation (24), the effective constitutive equation for the multiphase unit cell is obtained as:

$$\bar{\Xi} = \mathbf{L}^* \cdot \bar{\mathbb{E}} \tag{25}$$

where $\bar{\Xi} = [\bar{\boldsymbol{\sigma}}, \bar{\mathbf{D}}]^{\mathrm{T}}$ and $\bar{\mathbb{E}} = [\bar{\boldsymbol{\varepsilon}}, -\bar{\mathbf{E}}]^{\mathrm{T}}$. $\mathbf{L}^* = \begin{bmatrix} \mathbf{C}^* & \mathbf{e}^* \\ \mathbf{e}^{*\mathrm{T}} & -\boldsymbol{\kappa}^* \end{bmatrix}$. $\mathbf{C}^*$, $\mathbf{e}^*$, and $\boldsymbol{\kappa}^*$ are the effective elastic stiffness, piezoelectric, and dielectric matrices, respectively.

## 4. Numerical results

In this section, numerical examples of a fuzzy fiber composite with multiphysics phases are presented. The scope is to test the accuracy of the proposed multiphysics finite-volume and finite-element-based two-step homogenization scheme. The latter is typically regarded as the computational standard in the simulation communities.

**Table 1.** Properties of the epoxy matrix and graphene.

| | $E$ (GPa) | $\nu$ | $\kappa$ ($C^2/GNm^2$) |
|---|---|---|---|
| Epoxy | 3 | 0.3 | 3.098966E−02 |
| Graphene | 1100 | 0.14 | 6.109390E−02 |

The fuzzy fiber composites studied herein consist of the classical epoxy matrix, the PZT main fiber, and the carbon nanotubes walls made of graphene. While the epoxy matrix and graphene are isotropic, the PZT main fiber is transversely isotropic material. The properties of all the material phases are summarized in Tables 1 and 2. It should be mentioned that the effective properties of carbon nanotubes walls are transversely isotropic (Chatzigeorgiou et al., 2020) despite the fact that graphene is isotropic.

The determination of geometrical parameters (such as the thickness of the CNT interface and radii of the micro and main fibers), the volume contents of the CNTs (hollow microfibers made of graphene) and the PZT main fiber is of great importance to the overall properties of the fuzzy fiber composites. In this manuscript, the CNTs have an inner radius of $0.51nm$ and an external radius of $0.85nm$(Chatzigeorgiou et al., 2012). The diameter of the PZT main fiber is taken to be $100\mu m$. The length of the CNTs (namely the thickness of the nanocomposite coating layer) is assumed to be $25\mu m$. While the characteristic sizes of the main fiber and the nanocomposite interphase have been kept as constants, the volume fraction of the CNTs in the nanocomposite interphase and the overall fuzzy fiber volume fraction may vary.

### 4.1. Microscale homogenization: CNTs reinforced matrix

Figure 3 shows the cross-section of the nanocomposite interphase reinforced by radially aligned CNTs. It is assumed that the CNTs are perfectly straight and dispersed uniformly in the epoxy matrix. Due to the perfect orientation of the CNTs in the radial direction,

**Table 2.** Properties of the PZT main fiber.

| $C_{11}$ (GPa) | $C_{12}$ (GPa) | $C_{22}$ (GPa) | $C_{23}$ (GPa) | $C_{44}$ (GPa) | $C_{66}$ (GPa) |
|---|---|---|---|---|---|
| 131 | 74.24 | 148 | 76.2 | 35.9 | 25.3 |
| $e_{11}$ ($C/m^2$) | $e_{12}$ ($C/m^2$) | $e_{26}$ ($C/m^2$) | $k_{11}$ ($C^2/GNm^2$) | $k_{22}$ ($C^2/GNm^2$) | $k_{33}$ ($C^2/GNm^2$) |
| 10.99 | −2.324 | 9.31 | 2.081 | 3.984 | 3.984 |

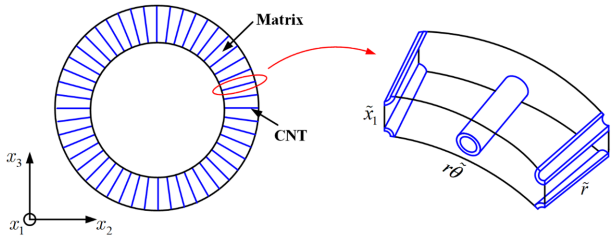


**Figure 3.** Cross-section of the nanocomposite interphase reinforced by radially aligned CNTs.

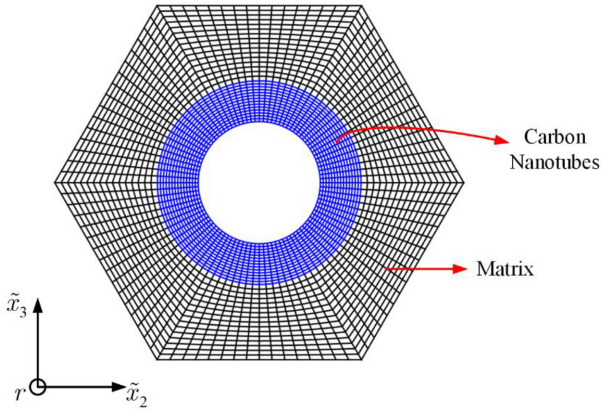


**Figure 4.** Discretization of repeating unit cell representative of nanocomposite interphase reinforced by CNTs. The hollow CNT fiber has an inner radius of 0.51*nm* and external radius of 0.85*nm*.

there is no drastic variation of material properties, local stress and strain (or electric field and electric displacement) fields in the pertinent direction. Therefore, the unit cell problem is reduced to a two-dimensional problem with the generalized plane strain constraint. It should be noted that at high CNTs content, the CNTs are typically not well distributed in the nanocomposite interphase, resulting in possible agglomeration of the carbon nanotubes (Chatzigeorgiou et al., 2020). To consider the agglomeration of the carbon nanotubes at the microscale, a three-dimensional unit cell analysis is required, which leads to the excessively large size of the global system of equations. Therefore, in this manuscript, such aspects are not considered due to the high computational cost.

In general, the microfibers are distributed randomly on the main fiber surface. For computational purposes, it is assumed a tetragonal or hexagonal array pattern of the microfibers. In this work, microscale homogenization is performed using the hexagonal arrangement of the CNTs, as shown in Figure 4. For clarity and simplification, the axes $(r, \theta, z)$ also are referred to as $(\tilde{x}_1, \tilde{x}_2, \tilde{x}_3)$. Due to the six-fold symmetry of the

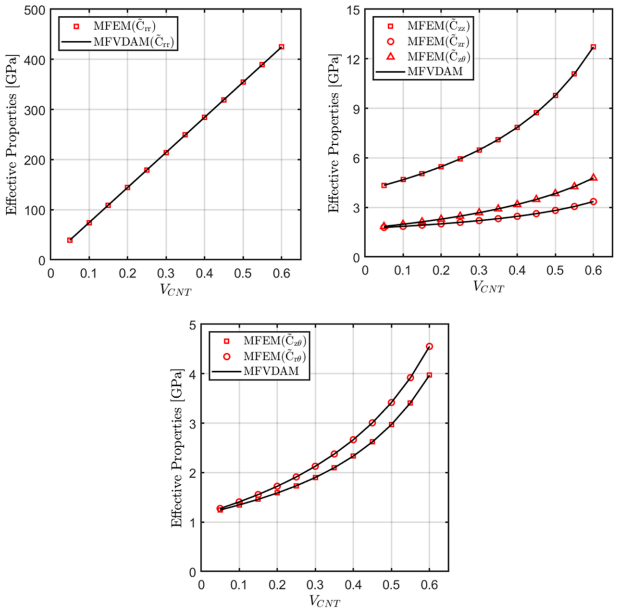


**Figure 5.** Comparison of homogenized mechanical properties of nanocomposite interphase as a function of CNT volume fraction.

hexagonal unit cell, the homogenized properties of the nanocomposites are transversely isotropic with the axis of the symmetry parallel to the radial (or microfiber axial) direction. In the multiphysics FVDAM theory, periodic boundary conditions of mechanical displacements, tractions, electric potentials, and electric displacements are directly applied on the opposite faces of the unit cell. To establish the complete generalized stiffness tensor of the nanocomposite, the unit cell problems are solved iteratively nine times by sequential imposition of only one unit macroscopic strain and electric field at a time with all other strain and electric field components equal to zero. As a result, the solution of the system of equation (17) thus equations (24) and (25) provides the nine components of the stresses and electric displacements, which correspond to the elements in the associated column in the effective generalized stiffness matrix.

Figure 5 shows the variations of the selected effective mechanical properties of the nanocomposite interphase as a function of the CNTs volume fraction ($V_{CNT}$) in the nanocomposite interphase. Figure 6 shows the variations of the homogenized dielectric properties as a function of the CNTs volume fraction. The multiphysics finite-element results generated based on the same unit cell architecture and mesh refinement are enclosed in the figures for comparison. As observed, the correlations of all the effective properties between the multiphysics FVDAM and FEM are remarkable. The value of the effective elastic stiffness $C_{rr}$ is significantly high

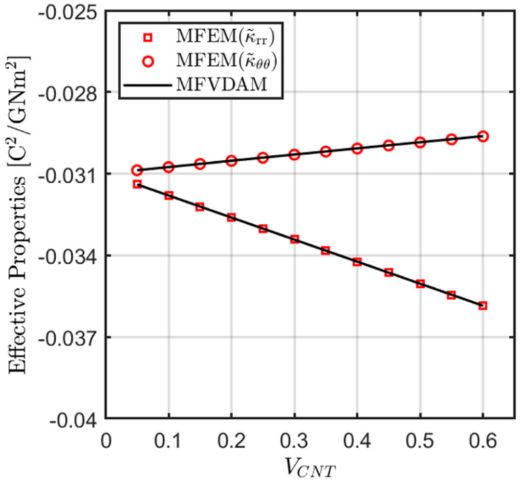


**Figure 6.** Comparison of homogenized dielectric properties of nanocomposite interphase as a function of CNT volume fraction.

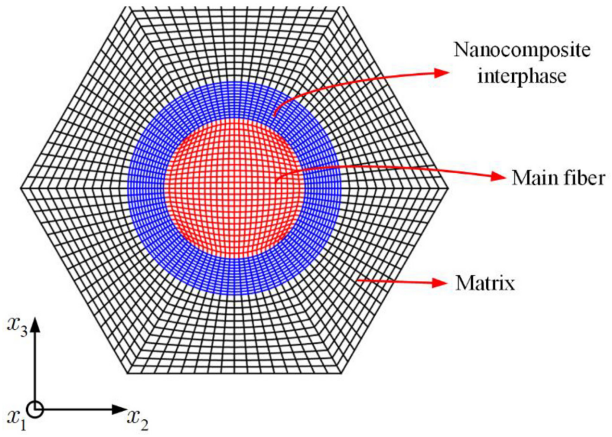


**Figure 7.** Discretization of repeating unit cell representing the overall fuzzy fiber composites. The diameter of the PZT main fiber is 100$\mu m$ and the length of CNTs is 25$\mu m$.

in the radial direction along which the CNTs are oriented.

### 4.2. Mesoscale homogenization: Fuzzy fiber-reinforced matrix

Having obtained the equivalent properties of the nanocomposite interphase, the homogenization of the overall fuzzy fiber composites can be conducted using either the MFVDAM or the MFEM again. The overall fuzzy fiber composites can be described directly in the Cartesian coordinates, where the actual composites are treated as a three-phase medium consisting of the main fiber, cylindrically orthotropic interphase layer, and the surrounding matrix. In the same spirit as the microscale homogenization, the mesoscale homogenization is performed on the hexagonal arrangement of the coated fiber with periodic boundary conditions, as shown in Figure 7. As before, the unit cell problems are solved iteratively nine times by sequential imposition of only one unit macroscopic strain and electric field at a time with all other strain and electric field components equal to zero.

It is worth mentioning that the homogenization of composites involving cylindrically orthotropic phases in the Cartesian coordinates necessitates expressing the effective properties of the nanocomposite interphase from cylindrical coordinates $(r, \theta, z)$ to the Cartesian coordinates $(x_1, x_2, x_3)$ according to the rotation formula equation (7). Figure 8 shows the selected components of the effective stiffness $C_{22}$ and $C_{44}$ in the Cartesian coordinates at three different CNTs volume fractions. It is observed that the nanocomposite interphase is a functionally graded monoclinic medium in the chosen coordinates whose effective properties rely

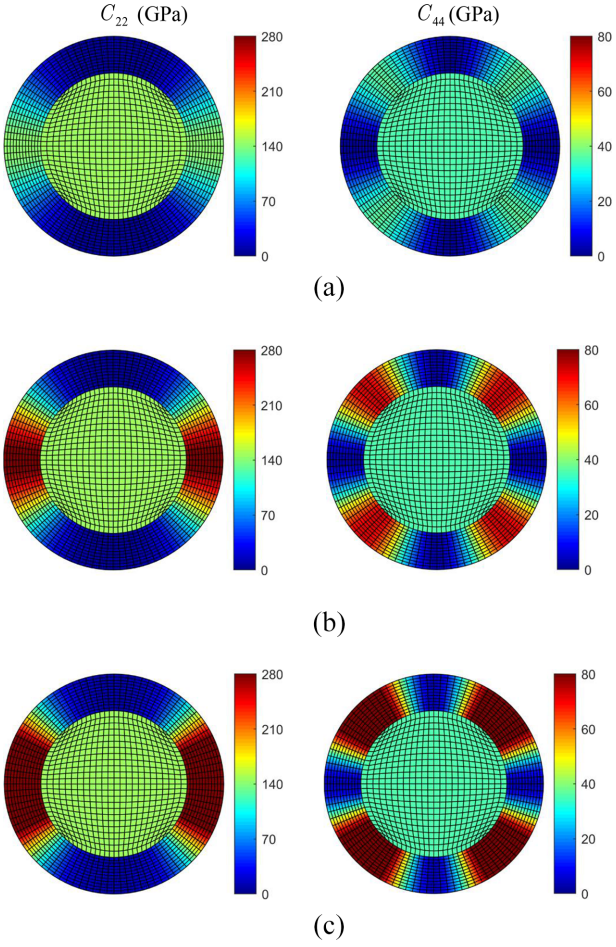


**Figure 8.** Comparison of the selected spatially-dependent stiffness components in fuzzy fiber in the global coordinate system, induced by the radially aligned CNTs at three different CNT volume contents: (a) $V_{CNT}$ = 20%, (b) $V_{CNT}$ = 40% and (c) $V_{CNT}$ = 60%.

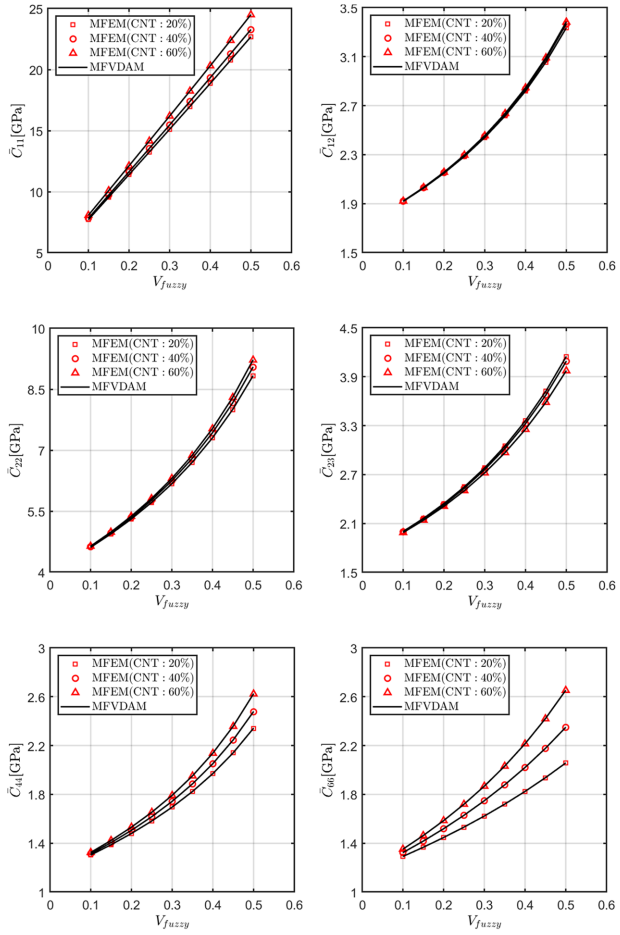


**Figure 9.** Comparison of homogenized mechanical properties of composites as a function of the overall fuzzy fiber volume fraction.

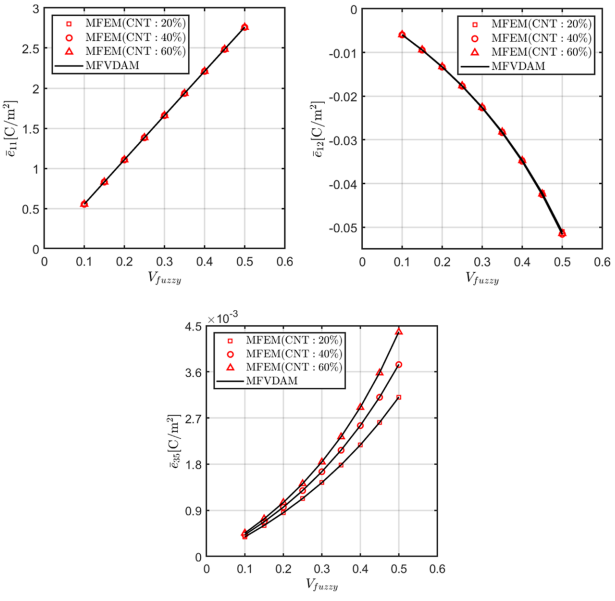


**Figure 10.** Comparison of homogenized piezoelectric properties of composites as a function of the overall fuzzy fiber volume fraction.

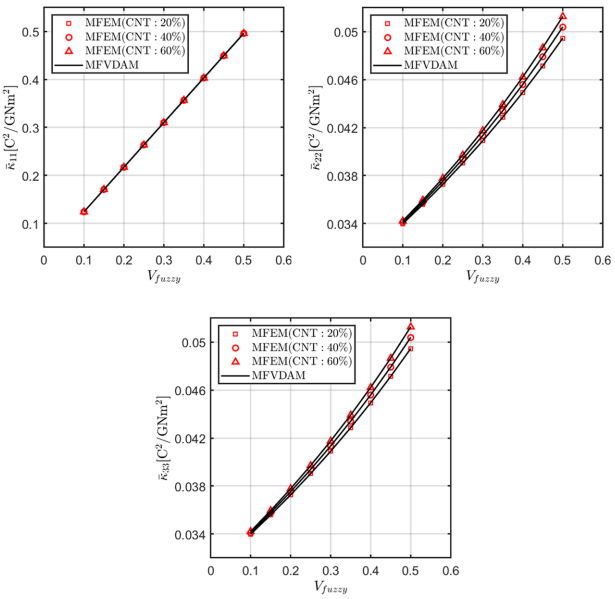


**Figure 11.** Comparison of homogenized dielectric properties of composites as a function of the overall fuzzy fiber volume fraction.

on the angular position. As a consequence of this spatial dependency, a special constitutive law with the rotated generalized stiffness detailed in Section 2 is introduced for elements or subvolumes that occupy the interphase.

Figures 9–11 summarize the results for the homogenized mechanical, piezoelectric, and dielectric properties of the fuzzy fiber composites as a function of the overall fuzzy fiber volume fraction at three different CNTs volume contents. Both the finite-element and finite-volume predictions are plotted in the figures for comparison, where excellent agreements are obtained for every case for the two homogenization schemes. It should be noted that the solution principles employed in the finite-volume and finite-element methods are substantially different even though both techniques require the classical discretization of the analysis domain and the formation of the local thus global stiffness matrices. While the finite-element method looks for the displacement electric potential fields that satisfy the governing differential equations (namely the stress equilibrium and Maxwell conservation equations) after the total potential energy is minimized, the finite-volume theory directly solves the strong form of the governing differential equations in each discretized subvolume in a volume-averaged sense. It should be noted that both the finite-element and finite-volume analyses are conducted using 2880 elements or subvolumes. A much finer mesh with 11,520 has also been used to perform the computations but doesn't yield different results, providing direct evidence for the accuracy of the

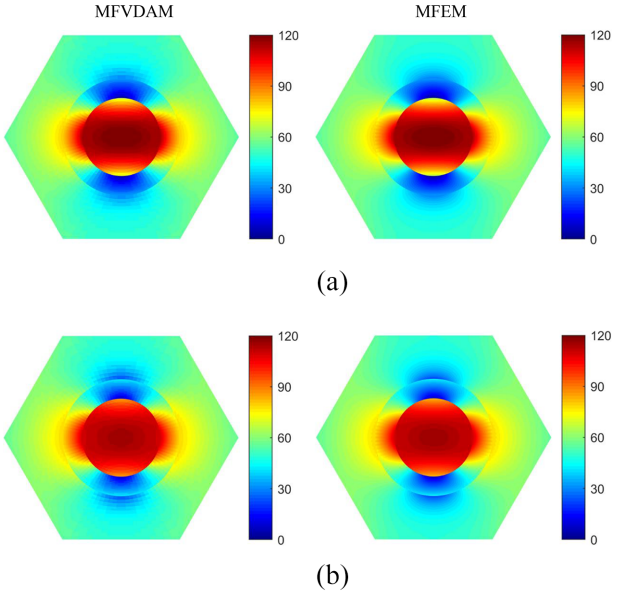


**Figure 12.** Comparison of the mesoscale stress field $\sigma_{22}$(MPa) generated by the multiphysics FVDAM and FEM methods with the imposition of only one macroscopic strain $\bar{\varepsilon}_{22} = 1\%$: (a) $V_{CNT} = 20\%$ and (b) $V_{CNT} = 60\%$.

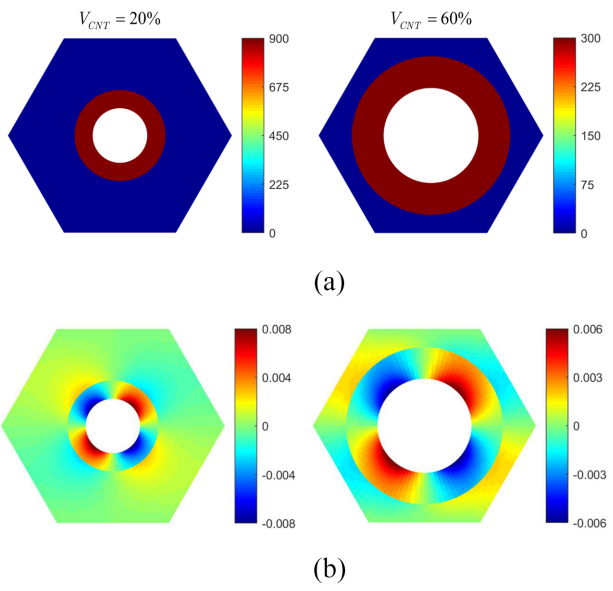


**Figure 13.** Micro-scale stress and electric displacement field recovery at the location $r = 50nm, \theta = 0$ generated by the multiphysics FVDAM for two different CNT volume fractions with the imposition of the same macroscopic strain $\bar{\varepsilon}_{22} = 1\%$. It should be noted that the overall fuzzy fiber volume fractions at the mesoscale are kept at 30%: (a) $\sigma_{22}$(MPa) and (b) $d_z(C/m^2)$.

generated results with the adopted level of mesh refinement. Using the selected mesh discretization, the computation of the complete set of homogenized properties for the overall fuzzy fiber composites takes about 443 and 47 s (averaged based on three runs) respectively for the MFEM and MFVDAM approaches, which were executed on a personal computer with Intel(R) Core (TM) i7-6600U @ 2.60 GHz 2.81 GHz, 8.0 GB memory, 64-bit Operating System, × 64-based processor.

### 4.3. Recovery of local fields

Compared to the mean-field homogenization methods in the literature, an important advantage of the developed multiphysics full-field homogenization methodologies is the ability to efficiently and accurately identify the local stress and electric fields at meso- thus microscales. In this subsection, to demonstrate the capability of the developed strategies for predicting the local fields distributions, the overall fuzzy fiber composite is subjected to the macroscopic strain $\bar{\varepsilon}_{22} = 1\%$. All other macroscopic strain components and electric fields are kept as zeros. The fuzzy fiber volume fraction is taken to be 30%.

The mesoscale stress $\sigma_{22}$ field distributions are obtained at two different CNTs volume contents, namely $V_{CNT} = 20\%$ and $V_{CNT} = 60\%$, generated using the MFVDAM and MFEM approaches in Figure 12. Overall, it is observed an excellent agreement between the MFVDAM and MFEM homogenization techniques. However, the MFEM seems to provide smoother stress distributions, particularly in the vicinity of the coating on the matrix side. This observation was expected since the MFEM results shown in Figure 12 are generated using the Serendipity biquadratic elements while the MFVDAM employs the second-order Legendre polynomial in the representation of the displacements and electric potentials. Another reason for the lack of smoothness of local fields in finite-volume theory is the fact that the continuity conditions connecting the adjacent subvolumes are enforced in a surface-averaged sense. Figure 13 depicts the micro-level stress and electric displacement field distributions at the point $r = 50nm$, $\theta = 0$ for two different CNT volume fractions $V_{CNT} = 20\%$ and $V_{CNT} = 60\%$. To generate the results in Figure 13, the strain and electric field at $r = 50nm$, $\theta = 0$ are retrieved from the mesoscale analysis and are then applied to the microscale unit cell. To avoid duplication, only finite-volume results are shown. It is observed that increasing the CNTs volume content tends to decrease the microscale stress field in the CNTs phase.

## 5. Discussion

The objective of this manuscript is to study homogenized and local field distributions of fuzzy fiber composites under electro-mechanical loading conditions. Indeed, micromechanical simulations of fuzzy fiber microstructures play an indispensable role in the development of novel material systems because they not only

can facilitate the identification and selection of candidate materials for specific applications but also the development and fabrication of engineered materials with target electro-mechanical properties, as well as optimization of the structural components in a multiscale setting. Presently, these complicated heterogeneous materials cannot be studied with the classical multiscale methodologies due to the presence of the cylindrically orthotropic material properties and multiphysics effects. It is worth mentioning that, in Cartesian coordinates of a standard unit cell, a cylindrically orthotropic material acts as a functionally graded material (see Figure 8) with anisotropic response (terms such as $C_{42}$ and $C_{43}$ are not zero). Hence in this contribution, two numerical homogenization techniques based on finite-volume and finite-element theories are presented to tackle the problems encountered in the modeling of fuzzy fiber composites. The two approaches predict essentially the same homogenized properties and local fields, providing good support for the generated results. Comparison against the experimental data is a worthwhile pursuit to further validate the modeling strategies for fuzzy fiber composites under electro-mechanical loading conditions. Unfortunately, sufficient experimental data for model validation is not readily available in the open literature since this material is still in the development stage.

It should be mentioned that the multiphysics finite-volume homogenization technique is an attractive alternative to the finite-element method, the latter of which is typically the computation standard in the literature. Both approaches are based on mesh discretization of unit cells into subvolumes/elements, two-scale expansion of the displacement fields involving the macroscopic and fluctuating contributions, and the formation of local/global system of equations. The solution principles, however, are fundamentally different:

A major difference between the finite-element and finite-volume based unit cell solution is the manner of satisfying local, and thus global, equilibrium and Maxwell conservation equations. Namely, while the minimization of the total potential energy in the finite-element approach leads to the ultimate satisfaction of the unit cell's global equilibrium and conservation with sufficient mesh refinement, the multiphysics finite-volume technique is based on strong form solution of the stress equilibrium and conservation equations in a volume-averaged sense at any level of mesh refinement.

Secondly, the finite-element method requires numerical integration of the local stiffness matrices. The finite-volume technique is semi-analytical in the sense that explicit expressions for the local stiffness matrices can be derived, hence an increase in computation efficiency.

Finally, in the finite-element technique, the continuity and periodicity conditions are applied only on the nodal displacements and electric potential whereas, in the finite-volume technique, continuity and periodicity conditions are enforced on both surface-averaged tractions/electric displacements and mechanical displacements/electric potentials.

## 6. Summary and conclusion

Fuzzy fiber composites are hierarchically reinforcing heterogeneous materials in which the main fibers are coated with radially aligned CNTs. Due to the complexity of the microstructures, two generalized zeroth-order asymptotic homogenization approaches, based on finite-volume and finite element micromechanics theories, have been proposed in order to evaluate the homogenized and local response of fuzzy fiber composites at different scales. The developed framework account for both the multiphysics piezoelectric effect and the cylindrical orthotropic material behavior at the phase level for the first time. A recursive multiscale analysis algorithm was developed wherein homogenized moduli (or local fields) obtained from the homogenization (or localization) analysis at one scale are used in the calculation of homogenized moduli (or local fields) at the next scale. New results are generated for a unidirectional fuzzy fiber composite considering PZT fibers enhanced by the CNTs which are embedded in the epoxy matrix. It is observed a good agreement between the MFVDAM and MFEM approaches. The present manuscript focuses on establishing new micromechanical models for fuzzy fiber composites with multiphysics effects which are extensively verified by the numerical examples. Parametric investigation with specific applications will be conducted in our future work to estimate the sensitivity of microstructural parameters and capture them with a first-order effect.

### Declaration of conflicting interests

The authors declared no potential conflicts of interest with respect to the research, authorship, and/or publication of this article.

### Funding

The authors received no financial support for the research, authorship, and/or publication of this article.

### ORCID iDs

Qiang Chen https://orcid.org/0000-0002-1623-8756
George Chatzigeorgiou https://orcid.org/0000-0002-7213-2980

### References

Aniskevich K and Starkova O (2021) Evaluation of the viscoplastic strain of high-density polyethylene/multiwall carbon nanotube composites using the reaction rate relation. *Mechanics of Composite Materials* 57: 577–586.

Aravand MA, Shishkina O, Straumit I, et al. (2016) Internal geometry of woven composite laminates with "fuzzy" carbon nanotube grafted fibers. *Composites Part A: Applied Science and Manufacturing* 88: 295–304.

Ay Z and Tanoğlu M (2020) The effect of single-walled carbon nanotube (SWCNT) concentration on the mechanical and rheological behavior of epoxy matrix. *Mechanics of Composite Materials* 56: 523–532.

Aziz S, Rashid SA, Rahmanian S, et al. (2015) Experimental evaluation of the interfacial properties of carbon nanotube coated carbon fiber reinforced hybrid composites. *Polymer Composites* 36(10): 1941–1950.

Cavalcante MAA, Marques SPC and Pindera M-J (2007) Parametric formulation of the finite-volume theory for functionally graded materials—Part I: Analysis. *Journal of Applied Mechanics* 74(5): 935–945.

Chatzigeorgiou G, Benaarbia A and Meraghni F (2019a) Piezoelectric-piezomagnetic behaviour of coated long fiber composites accounting for eigenfields. *Mechanics of Materials* 138: 103157.

Chatzigeorgiou G, Javili A and Meraghni F (2019b) Micromechanical method for effective piezoelectric properties and electromechanical fields in multi-coated long fiber composites. *International Journal of Solids and Structures* 159: 21–39.

Chatzigeorgiou G, Charalambakis N, Chemisky Y, et al. (2017) 1 - mathematical concepts. In: Chatzigeorgiou G, Charalambakis N, Chemisky Y, et al. (eds) *Thermomechanical Behavior of Dissipative Composite Materials*. Amsterdam: Elsevier. pp.1–36.

Chatzigeorgiou G, Efendiev Y and Lagoudas DC (2011) Homogenization of aligned "fuzzy fiber" composites. *International Journal of Solids and Structures* 48(19): 2668–2680.

Chatzigeorgiou G, Meraghni F, Charalambakis N, et al. (2020) Multiscale modeling accounting for inelastic mechanisms of fuzzy fiber composites with straight or wavy carbon nanotubes. *International Journal of Solids and Structures* 202: 39–57.

Chatzigeorgiou G, Seidel GD and Lagoudas DC (2012) Effective mechanical properties of "fuzzy fiber" composites. *Composites Part B Engineering* 43(6): 2577–2593.

Chen Q, Tu W, Liu R, et al. (2018a) Parametric multiphysics finite-volume theory for periodic composites with thermo-electro-elastic phases. *Journal of Intelligent Material Systems and Structures* 29(4): 530–552.

Chen Q, Wang G and Pindera M-J (2018b) Homogenization and localization of nanoporous composites - A critical review and new developments. *Composites Part B Engineering* 155: 329–368.

Chen Q, Chatzigeorgiou G and Meraghni F (2021) Hybrid hierarchical homogenization theory for unidirectional CNTs-coated fuzzy fiber composites undergoing inelastic deformations. *Composites Science and Technology* 215: 109012.

Chen Q and Wang G (2020) Computationally-efficient homogenization and localization of unidirectional piezoelectric composites with partially cracked interface. *Composite Structures* 232: 111452.

Christensen RM and Lo KH (1979) Solutions for effective shear properties in three phase sphere and cylinder models. *Journal of the Mechanics and Physics of Solids* 27(4): 315–330.

De Luca HG, Anthony DB, Greenhalgh ES, et al. (2020) Piezoresistive structural composites reinforced by carbon nanotube-grafted quartz fibres. *Composites Science and Technology* 198: 108275.

Dhala S and Ray MC (2015) Micromechanics of piezoelectric fuzzy fiber-reinforced composite. *Mechanics of Materials* 81: 1–17.

Hashin Z and Rosen BW (1964) The elastic moduli of fiber-reinforced materials. *Journal of Applied Mechanics* 31(2): 223–232.

He Z and Pindera M-J (2021a) Finite volume based asymptotic homogenization theory for periodic materials under anti-plane shear. *European Journal of Mechanics - A/Solids* 85: 104122.

He Z and Pindera M-J (2021b) Locally exact asymptotic homogenization of viscoelastic composites under anti-plane shear loading. *Mechanics of Materials* 155: 103752.

Isaeva AN and Topolov VY (2021) Comparative study on the performance of piezo-active 1–3-type composites with lead-free components. *Journal of Advanced Dielectrics* 11(5): 2160003.

Karger-Kocsis J, Mahmood H and Pegoretti A (2020) All-carbon multi-scale and hierarchical fibers and related structural composites: A review. *Composites Science and Technology* 186: 107932.

Kudimova AB, Nasedkin AV, Nasedkina AA, et al. (2021) Computer Simulation of composites consisting of piezoceramic matrix with metal inclusions and pores. *Mechanics of Composite Materials* 57: 657–666.

Kundalwal SI and Ray MC (2014) Effect of carbon nanotube waviness on the effective thermoelastic properties of a novel continuous fuzzy fiber reinforced composite. *Composites Part B Engineering* 57: 199–209.

Kundalwal SI, Suresh Kumar R and Ray MC (2013) Smart damping of laminated fuzzy fiber reinforced composite shells using 1-3 piezoelectric composites. *Smart Materials and Structures* 22: 105001.

Li R, Lachman N, Florin P, et al. (2015) Hierarchical carbon nanotube carbon fiber unidirectional composites with preserved tensile and interfacial properties. *Composites Science and Technology* 117: 139–145.

Lurie SA, Volkov-Bogorodskiy DB, Menshykov O, et al. (2018) Modeling the effective mechanical properties of "fuzzy fiber" composites across scales length. *Composites Part B Engineering* 142: 24–35.

Pindera M-J, Khatam H, Drago AS, et al. (2009) Micromechanics of spatially uniform heterogeneous media: A critical review and emerging approaches. *Composites Part B Engineering* 40(5): 349–378.

Qian H, Greenhalgh ES, Shaffer MSP, et al. (2010) Carbon nanotube-based hierarchical composites: A review. *Journal of Materials Chemistry* 20: 4751–4762.

Rao Y, Ban J, Yao S, et al. (2021) A hierarchical prediction scheme for effective properties of fuzzy fiber reinforced composites with two-scale interphases: Based on three-phase bridging model. *Mechanics of Materials* 152: 103653.

Song Q, Li K-Z, Li H-L, et al. (2012) Grafting straight carbon nanotubes radially onto carbon fibers and their effect on the mechanical properties of carbon/carbon composites. *Carbon* 50(10): 3949–3952.

Tsalis D, Chatzigeorgiou G and Charalambakis N (2012) Homogenization of structures with generalized periodicity. *Composites Part B Engineering* 43(6): 2495–2512.

Tu W and Chen Q (2021) Electromechanical response of multilayered piezoelectric $BaTiO_3$/PZT-7A composites with wavy architecture. *Journal of Intelligent Material Systems and Structures* 32(17): 1966–1986.

Yang H, Abali BE, Timofeev D, et al. (2020) Determination of metamaterial parameters by means of a homogenization approach based on asymptotic analysis. *Continuum Mechanics and Thermodynamics* 32: 1251–1270.

Yang H and Müller WH (2021) Size effects of mechanical metamaterials: A computational study based on a second-order asymptotic homogenization method. *Archive of Applied Mechanics* 91: 1037–1053.

Yildiz K, Gürkan Turgut F, et al. (2020) Fracture toughness enhancement of fuzzy CNT-glass fiber reinforced composites with a combined reinforcing strategy. *Composites Communications* 21: 100423.

Zhi J, Raju K, Tay T, et al. (2021a) Multiscale analysis of thermal problems in heterogeneous materials with direct $FE^2$ method. *International Journal for Numerical Methods in Engineering* 122(24): 7482–7503.

Zhi J, Raju K, Tay T-E, et al. (2021b) Transient multi-scale analysis with micro-inertia effects using direct $FE^2$ method. *Computational Mechanics* 67(6): 1645–1660.